Landslides DOI 10.1007/s10346-021-01778-3 Received: 24 May 2021 Accepted: 2 October 2021 © Springer-Verlag GmbH Germany, part of Springer Nature 2021

Dongri Song · Yitong Bai · Xiao Qing Chen · Gordon G. D. Zhou · Clarence E. Choi · Alessandro Pasuto · Peng Peng



Assessment of debris flow multiple-surge load model based on the physical process of debris-barrier interaction

Abstract Debris-flow impact load is one of the key parameters for design of engineering countermeasures. The multiple-surge load model is a remarkable progress in estimating the debris-flow impact load, which clearly delineates the contribution of each surge to the total impact load and the corresponding acting points. In order to better understand the impact process of channelized debris flow against flexible barrier, a series of medium-scale flume experiments with varying debris-flow volumetric solid concentration (0.40/0.50/0.55) were conducted. Especially, surge impact behavior is focused so that the predictability of the multiple-surge load model could be assessed. The flume and model flexible barrier were instrumented so that both the barrier dynamic response and the debris-flow properties (flow regime) could be correlated to facilitate the assessment. The results show that multiple-surge load model well predicts the total impact load. However, due to the simplification in the impact process, the interaction between the mobile phase (surge) and the deposited phase is ignored, resulting in discrepancy in the load distribution between the model prediction and experimental result. The remixing of deposited debris by the subsequent surges leads to downward momentum transfer to the lower section of barrier, which should be regarded as an adverse scenario of the design of flexible-barrier anchor capacity.

Keywords Debris flow \cdot Multiple-surge impact \cdot Load model \cdot Flexible barrier \cdot Load profile

Introduction

As a common geological hazard in mountainous area, channelized debris flow is characterized by its high mobility, multiple surges, and strong destructive power (Iverson 1997; Rickenmann et al. 1999; Shi et al. 2021). To protect human lives and properties under the threat of debris flows, various countermeasures have been developed, where steel-net flexible barrier is found effective in its functionality and efficient in construction and maintenance (Wendeler et al. 2007). Flexible barriers mitigate debris-flow hazards by intercepting the solid components of debris flow (coarse debris, boulders, and tree trunks) and draining debris materials to weaken the fluidity (Li and Zhao 2018; Wendeler et al. 2018). Nevertheless, there is still vagueness on the mechanism of debris flow-flexible barrier interaction, which hampers the establishment of accurate load models for engineering design.

The establishment of a rational debris-flow load model should be based on a full understanding of the kinematic and dynamic characteristics of debris flow itself (Kong et al. 2021). First of all, no matter what method is adopted to describe the movement of debris flow, identifying the flow regime and rheological properties is always the most important issue (Zhou and Ng 2010). Multiple surge is one of the important characteristics of debris flow in natural settings. The repeated loading action of surges sharply increases the destructive force and causes structural fatigue (Zanuttigh and Lamberti 2007; Zhou et al. 2018; Tan et al. 2020). At present, the understanding on multiple-surge debris-flow impact on flexible barrier is still superficial. Furthermore, the characteristics of multiple-surge debris flows indicate that there will be debris-flow deposits behind the barrier during subsequent debris-flow impacts. How the subsequent flows interact with the debris-flow deposits remains an open question. For example, the pore fluid pressure evolution within the deposits would affect the flow resistance of the overlying flowing surges and the static load on barrier. Thus, the state of debris-flow deposits behind the barrier is important for evaluating the impact load against flexible barrier.

This study first briefly reviews the existing single-surge and multiple-surge load models of debris flow. In order to evaluate the rationality of multiple-surge load model, impact experiments of multiple-surge debris flow with varying solid concentrations on a model flexible barrier are then carried out in a medium-scale flume. The kinematic and dynamic characteristics of multiple-surge debris flows during the impact process are captured. Furthermore, the changes in properties of debris-flow deposits during consolidation and its influence on the static load are investigated.

Load models of debris flow

Currently, various load models have been developed to estimate the impact force of debris flow on engineering countermeasures (Huang and Zhang 2020). To facilitate engineering design, hydrostatic model and hydrodynamic model are widely used due to their concise formulation (Hübl et al. 2009). The hydrostatic formula can be expressed:

$$F = \frac{1}{2}k\rho gh^2 w \tag{1}$$

where F is the debris-flow impact force (N), k is the hydrostatic pressure coefficient, ρ is bulk density of debris flow (kg/m³), g is acceleration of gravity (m/s²), h is the depth of debris flow (m), and w is the width of barrier (m). In contrast, the hydro-dynamic formula can be expressed:

$$F = \alpha \rho v^2 h w \tag{2}$$

where α is the hydrodynamic pressure coefficient, and ν is frontal velocity (m/s). Currently, the recommended α value by the Geotechnical Engineering Office of Hong Kong is 1.5 (GEO 2020).

Note the above two models only consider single-surge impact. More importantly, they are over-simplified. The load of debris flow on barrier is composed of two parts: dynamic load and static load (Faug 2015; Song et al. 2017). Models considering hydrostatic and hydrodynamic components can be found in Armanini et al. (2020) and Song et al. (2021a, b). Such models improve the rationality of load calculation. However, natural debris flows always demonstrate characteristics of multiple surges which are ignored by the above models.

Based on the observation of debris-flow impact from Illgraben monitoring site and laboratory experiments, Wendeler et al. (2019) proposed a multiple-surge load model. For the first impact (Fig. 1a), the impact load F is expressed as a combination of both the dynamic and static components:

$$F = \alpha \rho v^2 h w + \frac{1}{2} k \rho g h^2 w \tag{3}$$

For subsequent debris-flow impact (Fig. 1b), the impact load is expressed:

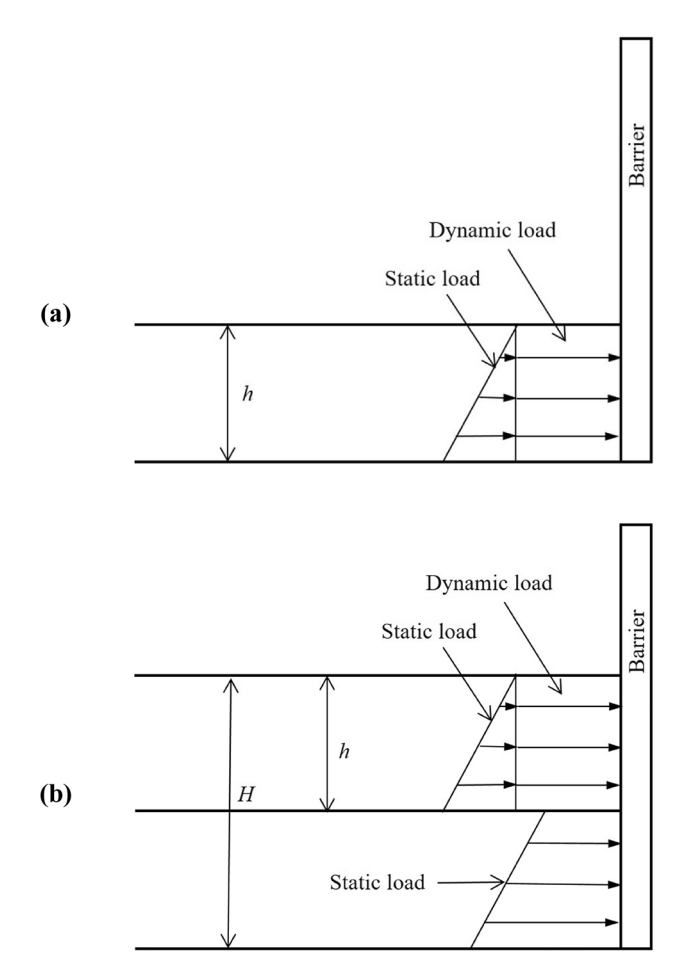


Fig. 1 Multiple-surge debris-flow loading scenarios. **a** First surge impact when barrier is empty. **b** Subsequent surge impact, loading contributed by both the deposited and flowing debris (Kwan 2012; Wendeler et al. 2019)

$$F = \alpha \rho v^2 h w + \frac{1}{2} k \rho g H^2 w \tag{4}$$

In Eq. 4, *H* represents the total height (m) of both preceding static deposit and the flowing debris (Fig. 1b).

There are several implicit assumptions for the multiple-surge load model: (1) The two-phase debris flow is regarded as singlephase fluid, and thus the regulation of pore fluid pressure to the dynamics is neglected. (2) The debris material behind the barrier is divided into two parts. One is the mobile phase (with flow depth h) and the other is the deposited phase. There is no interaction between the mobile phase and deposited phase (Fig. 1b). (3) The runup process of debris is neglected and the impact load concentrates in the area of flow depth h. This is proved to be true in the flows with vertical jet-up, as the runup part has velocity (momentum) parallel to the barrier face (Song et al. 2021b), (4) The impulse load of boulders has to be considered separately (Kwan 2012) but could be neglected in design of flexible barrier (Song et al. 2019a). Under the assumption that there is no interaction between the mobile phase and deposited phase, the dynamic load is exerted by the mobile phase and static load is exerted by both the mobile phase and deposited phase (Kwan 2012; Wendeler et al. 2019).

Modeling debris-flow impact using a medium-scale flume

Scaling principle

It is essential to consider the similarity between model experiments in reduced-scale flume and natural debris flows. Due to the low frequency and complicated channel topography of natural debris flows, it is difficult to carry out systematic research of debris-barrier interaction on site. Small- and medium-scale physical experiments have long been criticized by the scale effect, i.e., the effects of liquid-phase viscosity in debris flow is amplified and pore fluid pressure dissipates much faster (Iverson 2015). Yet, the experimental conditions of small- and medium-scale physical experiments are fully controllable, highly repeatable, easy to implement instruments, and are currently the most widely adopted approach to study the microscopic mechanisms of debris-flow movement and its interaction with structures (Armanini et al. 2020; Song et al. 2021b).

To evaluate the influence of scale effect, in this study, a series of dimensionless numbers are adopted to describe the macroscopic and microscopic flow regime of debris flow. Dimensionless numbers are widely used in the design of debris-flow experiments for consideration of dynamic similarity between models and prototype debris-flow events (Iverson 2015). The Froude number *Fr* is widely used for the dynamic similarity of fluids with free surfaces, macroscopically characterizing the relative importance of fluid inertial and gravitational forces (Choi et al. 2015):

$$Fr = \frac{v}{\sqrt{gh\cos\theta}} \tag{5}$$

where θ is the slope inclination (°).

The inertial-pore fluid pressure dissipation time ratio $N_{\rm p}$ quantifies the relative length of time scale that the debris flows along the slope under gravity and the vertical dissipation time scale of pore fluid pressure (Iverson 2015):

$$N_{\rm p} = \frac{\sqrt{l/g}}{\mu h^2/KE} \tag{6}$$

where l is the characteristic length of flow (m), μ is the dynamic viscosity of liquid phase (Pa·s), K is the intrinsic permeability of solid phase (m²), and E is the compression modulus of solid phase (Pa).

The Bagnold number $N_{\rm B}$ represents the relative magnitude of the inertial stresses caused by the instantaneous collision of particles and the liquid viscous stresses:

$$N_{\rm B} = (\frac{C_{\rm s}}{1 - C_{\rm s}}) \frac{\rho_{\rm s} \dot{\gamma} d_{50}^2}{\mu} \tag{7}$$

where C_s is the volumetric solid concentration of debris flow, ρ_s is particle density (kg/m³), $\dot{\gamma}$ is shear rate (1/s), and d_{50} is the median size of particles (m).

The Savage number N_S characterizes the ratio of instant grain collision stresses and sustained grain contact stresses (Savage 1984):

$$N_{\rm S} = \frac{\rho_{\rm s} \dot{\gamma}^2 d_{50}^2}{\sigma - p} \tag{8}$$

where σ is the basal normal stress (Pa) and p is pore fluid pressure (Pa). When basal stress measurement is available, σ -p in the denominator of Eq. 8 represents the effective stress of debris flow.

Model setup

The medium-scale concrete flume consists of a gate at the upstream, a linear transportation zone, and a model flexible barrier at the downstream (Fig. 2a). The distance from gate to model barrier is 7.15 m, and the width between two sidewalls is 0.7 m for simulating channelized debris flows. The inclination of flume is constant at 12° which is a major limitation of this test setup. This relatively low inclination enhances the basal flow resistance and limits the maximum solid concentration of debris flow to about 0.60. While debris flows with even higher solid concentration are featured with complicated solid–fluid interaction and should be the focus of debris-flow impact research. Maximum solid concentration of 0.55 is adopted in this study (see the section "Test program and procedure"). The section upstream of the gate is used as a container to store debris materials. Upon uplift of the gate, the debris can be released to model a dam-break failure.

Model flexible barrier

Due to the complicated elasto-plastic loading behavior, it is rather difficult to scale down the properties of a prototype flexible barrier into the model scale (Ng et al. 2016). To reveal the key interaction between debris flow and flexible barrier, a simplified model flexible barrier is adopted. The 0.45 m high and 0.7 m wide model barrier consists of a net and four steel strand cables which are isometrically installed on the net with a spacing of 0.15 m (Fig. 2c). The model barrier is installed adjacent to basal sensing module 2 (Fig. 2a). The net is made of high-density polyethylene with mesh opening of 5 mm. When debris flow impacts the model barrier, the debris first contacts the net surface, then the

net transfers the impact force to the cable. Slack is provided in the net to ensure the debris impact load can be fully transferred to the horizontal cables.

As reported by Song et al. (2019b), majority (>90%) of the debris total (potential and kinetic) energy is actually dissipated in the process of internal and boundary shearing of debris flow itself. The key function of a deformable barrier is to provide enough space for the debris to fully mix and deform. Thus, in this barrier setup, flexibility provided by the energy dissipating elements and deformable net is replaced by a 0.2 m prescribed deformation in the horizontal cable, i.e., the length of each horizontal cable is set as 0.9 m. Both sides of the cables are connected to the concrete side walls using expansion bolts (for modelling of anchor foundation in prototype). A side by side comparison of the key characteristics between prototype flexible barrier and model barrier of this study is listed in Table 1.

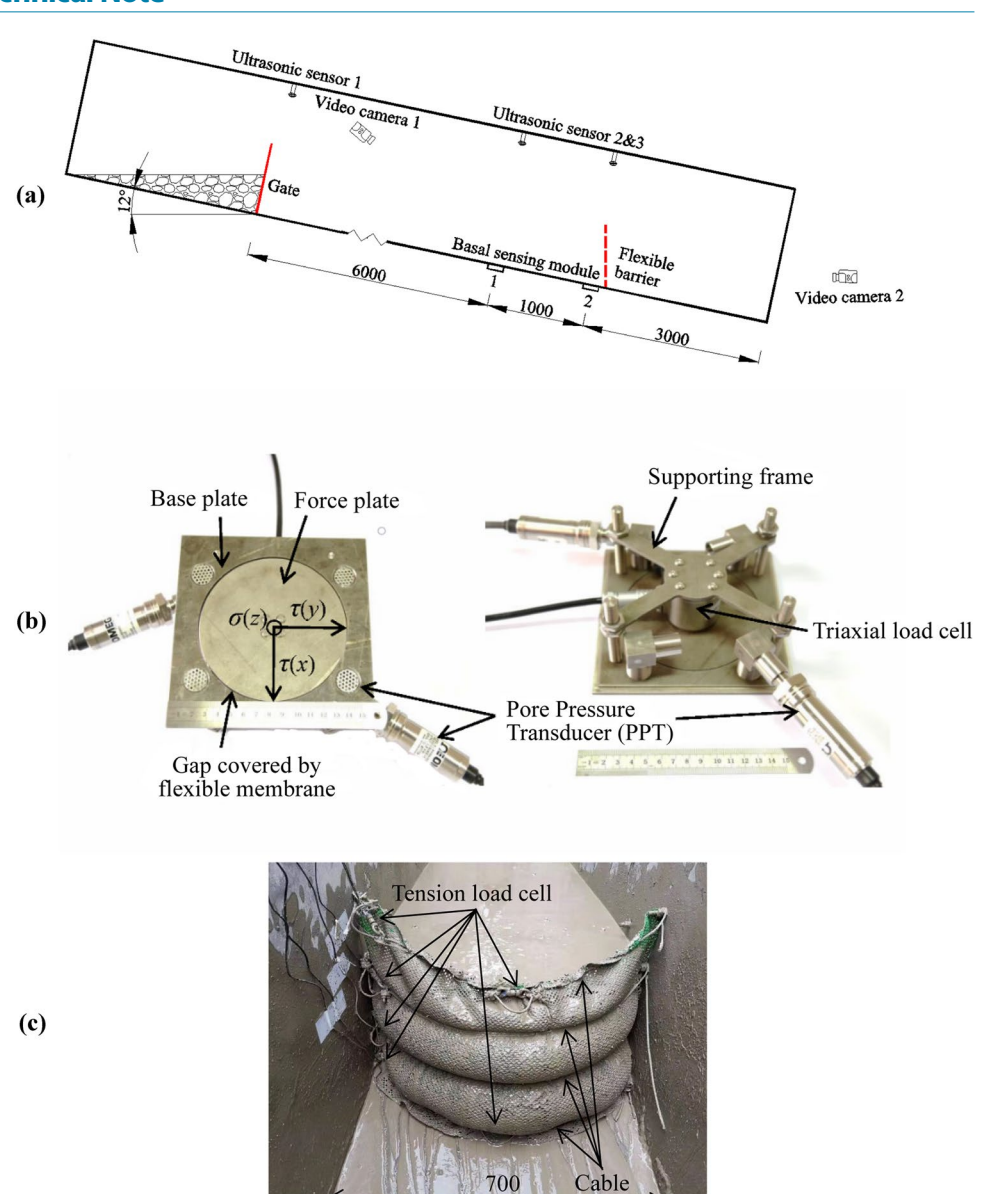
Instrumentation

Appropriate measurement of debris-flow properties is the key to understand the complicated debris-barrier interaction and to assess the existing load models. The normal/shear stresses and pore fluid pressure are measured by two basal sensing modules (Fig. 2b) which are installed into and with their surface flush with the bed of flume (Fig. 2a). Basal sensing module consists of a triaxial load cell for measurement of basal normal stress and shear stress (along the flow direction), and a pore pressure transducer (PPT) for measurement of pore fluid pressure. Unlike normal stress, the measurement of shear stress has greater technical difficulty. There is a finite gap between the base plate and the force plate, which is covered with a flexible membrane (Fig. 2b). It avoids the entry and clogging of fine particles into the gap. On the other hand, the thin membrane provides negligible stiffness to the system so that guarantees the effectiveness of shear force transmission. The open end of PPT is covered by a 0.4 mm steel mesh, which prevents entry of coarse particles. Before the start of each experiment, to ensure the accuracy of pore fluid pressure measurement, water is injected into the pore pressure transducers through the steel mesh to its saturation. The two modules are installed at 6 m and 7 m downstream of the gate (Fig. 2a), respectively.

The flow depth of debris flow is measured by ultrasonic distance sensor. A total of three ultrasonic sensors are used, which are installed at the gate and directly above the two basal sensing modules. The ultrasonic sensor located at the gate serves as a trigger to determine the moment of debris-flow release. Video cameras are installed upstream and downstream of the model flexible barrier (Fig. 2a) to record the impact, filling, and overflow (if any) processes.

Six miniature tension load cells are installed on the four cables of model barrier to record the tensile force induced by debris impact. The top cable and the bottom cable are installed with one load cell close to the side wall and one in the middle (Fig. 2c), respectively. The purpose of two load cells on one cable is to verify the circular profile assumption (see Fig. 5) under distributed loading. The upper intermediate cable and lower intermediate cable are installed with one load cell close to the side wall.

Fig. 2 Model setup and instrumentation. a Flume setup. The model flexible barrier is installed 150 mm behind basal sensing module 2. b Up side and bottom side of basal sensing module. c Model flexible barrier setup. All units in mm



Debris flow material

The granular material used in this series of experiments is taken from the debris-flow deposits in the Jiangjia Gully, near the Dongchuan Debris Flow Observation and Research Station (DDFORS). The coarse particles in the deposits are removed using a 20 mm × 20 mm steel mesh. The particle size distribution of the material, with median particle size 2.84 mm and specific gravity 2650 kg/m³, is shown in Fig. 3. After sieving, the relative proportion is clay:silt:sand:gravel = 2.0:6.5:32.7:58.8. Removal of coarse particles increases the percentage of fine particles (clay and silt), and this would result in a higher pore fluid pressure and low

flow resistance in the modelled debris flow. Median particle size 2.84 mm means that majority of the particles are smaller than the mesh opening (5 mm). However, effective clogging forms when the opening is 4–6 times of the particle size. In this sense, majority of the particles would be clogged by the net.

There is a certain amount of fine particles (clay and silt) in the mechanical composition of debris flow. These fine particles, combined with water, form a solid-liquid unsorted slurry, which is of great significance to the movement of debris flow (Fei et al. 1991). The slurry is an inseparable body of debris flow, where the water and fine particles inside have the same kinetic characteristics (through viscous drag, buoyancy, and virtual mass forces, Pudasaini 2012).

Table 1 Side by side comparison on debris-barrier interaction between prototype and model

Key characteristics	Prototype	Model
Debris material	Clay to boulders up to meter level	Less than 20 mm, with median particle size 2.84 mm
Barrier deformation	With brake elements, elasto-plastic	Prescribed 0.2 m, elastic
Permeability of barrier net	High or low, depending on particle gradation Typical net opening: 100–300 mm Median particle size: mm to dm	Low, due to particle clogging Net opening: 5 mm Median particle size: 2.84 mm
Energy dissipation	> 90% by internal and boundary shearing, others by brake elements	About 100% by internal and boundary shearing
Peak impact load	Attenuated by large deformation and debris pass- through	Close to that of rigid barrier
State of static debris	Active or at rest, depending on the amount of deformation and degree of liquefaction	At rest. See the section "Assessment of load model based on the state of deposits"

Obviously, the threshold value between solid and fluid phase varies with flow regime, i.e., in fast-flowing state, larger particles would move in-phase with the fluid and be regarded as slurry. In the field observation at DDFORS, it was found that the solid mass content of particles < 2 mm generally does not vary with the total solid concentration (about 680 kg/m³, Fei et al. 1991), indicating that particles < 2 mm could be regarded as slurry. In this study, the maximum particle size of the debris-flow slurry is 1.2 mm (as suggested by Cui et al. 2005). Given the fine material below 1.2 mm is considered as part of liquid phase, the new median particle size is 4.30 mm (Fig. 3).

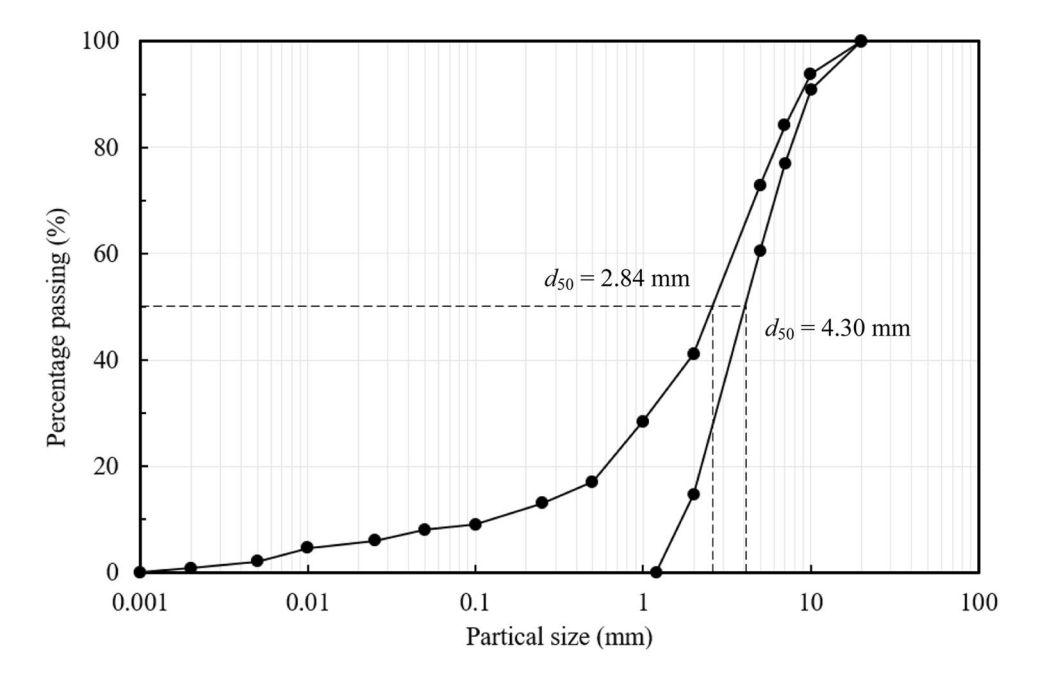
Test program and procedure

In order to study the impact of debris flows with different flow characteristics on flexible barrier, the volumetric solid concentration

(including the fine particles with particle size smaller than 1.2 mm) is set to 0.40, 0.50, and 0.55, covering a dilute to relative dense flow regime. The corresponding bulk densities are 1651, 1817, and 1880 kg/m³, respectively. Based on the rheological tests on debris-flow slurry in Jiangjia Gully (Yang et al. 2013), the viscosities are determined as 0.18, 0.40, and 0.54 Pa·s, respectively. In order to study the impact characteristics of debris flow under multiple surges, each experimental series is designed with three releases, and the volume of a single release is 0.15 m³. Details of the test program are summarized in Table 2. By adopting a concrete flume bed, this study does not consider the entrainment of completely consolidated materials of antecedent debris flow events; while the entrainment of loose deposits of these three surges has to be considered.

Once the model is prepared, the configured debris-flow mixture is loaded behind the gate and is repeatedly stirred to ensure the

Fig. 3 Particle size distribution of debris flow material



solid-liquid mixture remain well mixed. Before the gate is uplifted to release the first 0.15 m³ of debris, the flume bed is manually wetted using clear water (without running water on flume bed), and the data acquisition system and video cameras are switched on. After impacting the flexible barrier, the debris material accumulates behind the barrier and the deposit continues to drain and consolidate. It takes about 0.5 h for the second release and another 0.5 h for the third release. The stress change and pore fluid pressure dissipation during the consolidation process are recorded. After completion of the three debris-flow releases, the data acquisition system keeps recording for another 3.5 h to ensure that detailed consolidation information is collected. The sampling rate for the impact stage is set to 1000 Hz and is manually changed to 1 Hz for the consolidation stage.

Results and interpretation

Characterization of incoming flow regime

The basal normal stress/shear stress/pore fluid pressure and flow depth during the three releases of test with 0.50 solid concentration are shown in Fig. 4. The pore fluid pressure is roughly equal to the normal stress, indicating a fully liquefied state with no effective stress. The recorded data points of pore fluid pressure fluctuate, which is caused by the interaction between solid and liquid phases. While the fluctuation in normal and shear stresses reflects the frequent collision of solid particles. The recorded shear stress is roughly proportional to the normal stress. In Fig. 4c, the sensors record the reflected wave induced by the barrier. The wave moves upstream and thus the recorded shear stress goes below zero.

The deduced Froude number (Fr) values are between 1 and 5 and decrease with increasing solid concentration (Table 2). The change of inertial-diffusional time scale ratio ($N_{\rm p}$) values with the debris-flow surges is not significant, but as the solid concentration increases, the $N_{\rm p}$ value decreases significantly. This is because the vertical drainage time scale of the debris-flow material increased significantly with the increase of solid concentration. Thus, the $N_{\rm p}$ value can be used to qualitatively describe the drainage capacity of debris materials with different solid concentration. The Bagnold number ($N_{\rm p}$) values are between 3 and 18 and decrease with

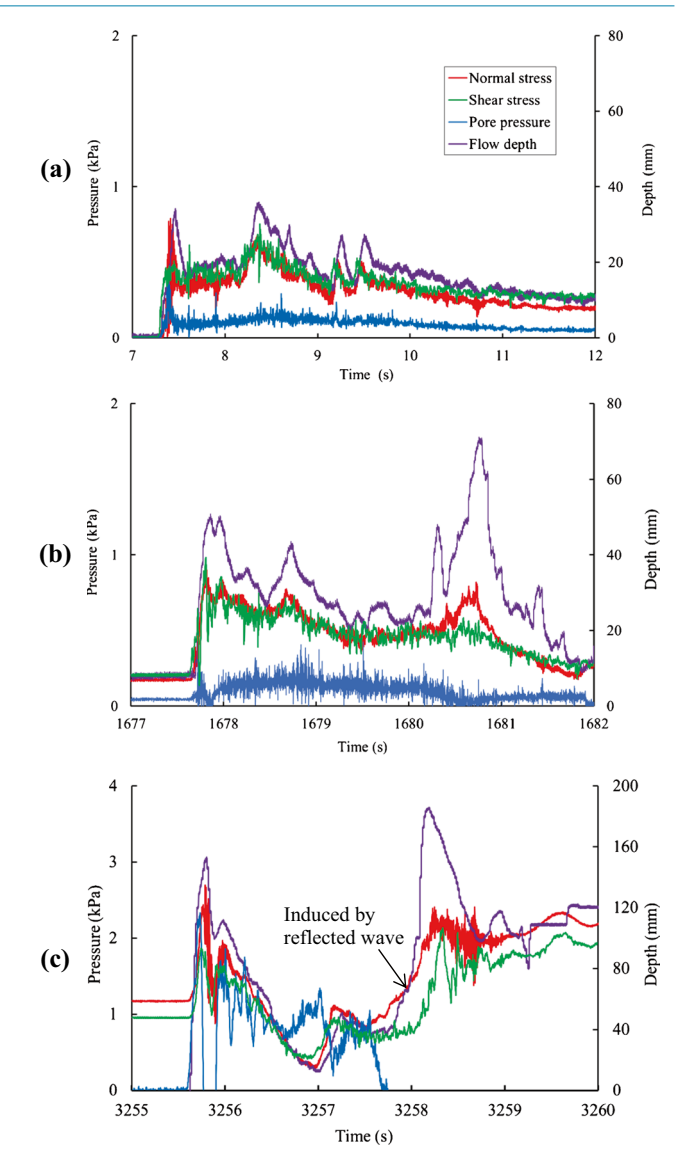


Fig. 4 Characterization of flow regime at basal sensing module 1 for test 50: $\bf a$ 50–1, $\bf b$ 50–2, and $\bf c$ 50–3

Table 2 Test program and characterization of flow regime

Test ID	Solid concentration (C _s)	Density ρ (kg/m³)	Fluid viscos- ity μ (Pa·s)	Velocity v (m/s)	Flow depth h (mm)	Froude number (Fr)	Inertial-diffusional time scale ratio (N _p)	Bagnold number (N _B)	Savage number (N _S)
40–1				2.33	24	4.8	1.2×10 ⁻¹	17.9	∞
40–2	0.40	1651	0.18	2.44	33	4.3	6.5×10^{-2}	13.7	∞
40–3				2.00	33	3.5	6.5×10 ⁻²	11.2	∞
50–1				2.00	33	3.5	2.4×10 ⁻³	7.5	∞
50–2	0.50	1817	0.40	2.22	49	3.2	1.1×10^{-3}	5.6	∞
50–3				2.17	49	3.1	1.1×10^{-3}	5.4	∞
55–1				0.41	17	1.0	1.8×10 ⁻³	2.7	∞
55–2	0.55	1880	0.54	2.22	58	2.9	1.6×10 ⁻⁴	4.3	∞
55–3				2.04	58	2.7	1.6×10 ⁻⁴	3.9	∞

increasing solid concentration. With $N_{\rm B}$ < 200 (Iverson 1997), the viscous stress dominates over the collisional stress. Since there is no effective stress in the experimental debris flows (even for those with 0.55 solid concentration), Savage number ($N_{\rm S}$) approaches infinity. Except the Savage number, which adopts the measurement of effective stress from the flume bed (Nagl et al. 2020), the range of dimensionless numbers of this study generally falls within the range of natural debris flows (Iverson 1997), so the similarity to the real debris flow is guaranteed. Detailed flow regime information is summarized in Table 2.

Impact kinematics

The impact processes of multiple surges against flexible barrier captured by the upstream video camera can be viewed in the Supplementary video. For the first surge, when the debris is released, a high surge front approaches the barrier with a uniform tail. After the surge front impinges on the barrier, a reflected wave is formed, which collides with the subsequent flow and an intense breaking wave is formed. At the same time, a small amount of debris passes through the barrier net. The amount of debris passing through the net decreases with increasing solid concentration. Due to the high flow resistance, the first surge of 0.55 solid concentration reaches the barrier base with limited frontal velocity and flow depth (Table 2) and fails to impose effective impact onto the barrier (see Fig. 8a).

In the two subsequent surges, the surge fronts run over the deposit of previous surge. The two-phase flow fronts are characterized as obvious jump with sharp change in flow depth through the jump interface, similar to the hydraulic jump phenomenon. The resulting frontal flow depth is higher than that of the first surge (Table 2). The subsequent surges demonstrate obvious mixing process with the deposited debris in front of the barrier, and this will be analyzed in combination with the basal measurement in the section "Evolution of basal stresses and pore fluid pressure." At the same time, a small amount of debris starts to run up along the barrier face and splashes out of the barrier. Owing to the limited volume of debris material, steady overflow is not formed. The amount of splash-out in the third surge is higher than that in the second surge. Due to the clogging of particles within the net opening, the amount of debris passing through the net is negligible.

It should be noted that, due to the continuous filling after the flow front impact of each surge, the final deposition height at the barrier is much higher than the flow depth. For example, in the 0.50 solid concentration impact, flow depth of the first surge of is 33 mm, yet the final deposition height is as much as 150 mm (see Fig. 10b). This deposition depth has to be considered in the calculation of total impact load of the second surge (Eq. 4).

Cable force and normal impact force

In order to calculate the normal impact force (normal to the barrier face) of debris flow on flexible barrier, the load model (relationship between cable axial tension force and flow impact force) proposed by Song et al. (2018, Fig. 5) has to be briefly introduced. The impact

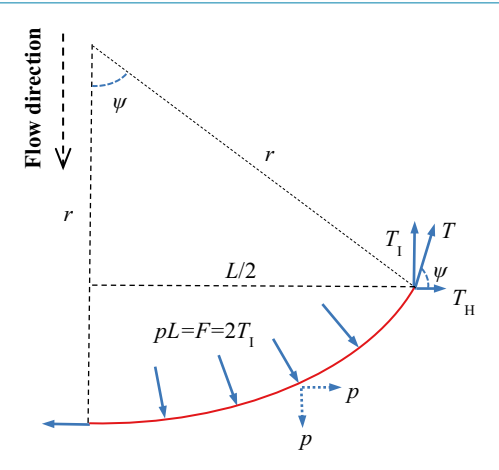


Fig. 5 Schematic diagram of the relationship between axial tension force and flow impact force of the cable (Song et al., 2018)

pressure of fluidized debris flow on the net can be regarded as a uniform load p. Under the uniform load, the flexible barrier bulges and the horizontal cables form a circular profile, where the cable force T remains unchanged along the arc of the circle (Fig. 5). The normal impact force F on one cable is in balance with the component of cable force T along the flow direction:

$$F = pL = 2T\sin\psi \tag{9}$$

where ψ is the deflection angle (°) and can be derived based on a chord length of L=0.7 m and an arc length of 0.9 m. To verify this load model, as introduced in the section "Instrumentation," two tension load cells are installed at different locations on the top and bottom cables (Fig. 2c). Experimental results demonstrate that the measured cable forces at different locations of one cable are close with each other. Therefore, the assumption of a circular profile under uniform load is appropriate.

Figure 6 a shows the time history of cable forces under multiple-surge impact with solid concentration of 0.40. Figure 6 b-d show the detailed characteristics of the normal impact force on the cable during the three surge impacts. Each surge impact is highly transient and followed by a quasi-static consolidation stage. The first two consolidation stages last about 0.5 h and the third lasts about 3.5 h (not fully shown in Figs. 6-8, further see Fig. 11). The lower intermediate cable (blue line) has the highest cable force (Fig. 6a) which is consistent with the results of a deformable flexible barrier by Song et al. (2018). While the top cable (red line) is characterized with the lowest cable force. The bottom cable (green line) has a higher initial value and is overtaken by the upper intermediate cable (black line) in the latter surge impacts. This is because the bottom cable is gradually buried by the static debris and is not further subjected to the dynamic impact of flowing debris.

As can be seen from Fig. 6b–d, the impact-induced force fluctuation lasts for about 3–4 s and then approaches static state. The total normal impact force (summation of normal impact force on the four cable, brown line) is consistent with the evolution of

impact force of each cable. The comparison of three surge impacts indicates that the peak impact load of the second impact almost doubles from the first impact, but increment of the third impact is minor. In addition, as the impact sequence proceeds, fluctuation of the impact force tends to be mild. The mild fluctuation of impact force implies the control of static deposit by previous surges in dissipating the kinetic energy. The experimental results of 0.50 and 0.55 solid concentration series demonstrate similar characteristics (Figs. 7 and 8). Note there are only two effective impacts in 0.55 solid concentration tests (Fig. 8).

Assessment of multiple-surge load model and discussion

Assessment based on total impact force

Figure 9 shows the comparison between the measured total impact force and the calculated values (with dynamic pressure coefficient α =1.5 and static pressure coefficient k=1) based on the multiple-surge load model (Fig. 1, Eqs. 3 and 4). The dotted diagonal line in the figure indicates the measured values well match the theoretical values predicted by the model. For surges with solid concentration 0.50, the peak loads under the successive impacts are close to the theoretical prediction. For surges with solid concentration 0.40, the peak loads are slightly under-predicted. For surges with solid concentration of 0.55, the peak loads are slightly over-predicted. This reflects the effects of debris-flow property (solid concentration and related energy dissipation mechanisms) on the distinct impact response. In terms of prediction in total impact force, the multiple-surge load model generally works well.

Assessment based on cable load profile

It is the horizontal cables that transfer the debris impact pressure to the deep force-bearing stratum through anchors. Thus, the bearing capacity of anchors is the key component of debris-flow flexible barrier design, and this is further verified in this section. Figure 10 shows the load profile of flexible barrier cable at the moment of peak force. In Fig. 10, the abscissa represents the normal impact force and the ordinate represents the height of flexible barrier. The four cables are located at 0.00, 0.15, 0.30, and 0.45 m, respectively. Terms h_1 , h_2 , and h_3 represent the incoming surge-flow depth and the dashed lines represent the position of the surge flow upon impact. Note the height (thicker than the flow depth) between surges denotes the gradual deposition of debris after the frontal impact, which only contributes to the static load in Eq. 4. The measured peak load distribution shows similar load profile (Fig. 10). Specifically, for the third surge impact, the height of the mobile layer is close to the upper intermediate cable, and therefore the maximum cable force should appear on it. However, the measured result shows that the maximum load stays on the lower intermediate cable. This is contradictory to the prediction of the multi-surge load model (Fig. 1).

To explain this discrepancy, we further explore the model assumption (see the section "Load models of debris flow") and experimental observation. The multi-surge load model assumes that the flowing layer and the deposited layer do not interact with each other, therefore the dynamic load is completely determined by the flowing layer (Fig. 1). However, it is found in the experiment that the subsequent surge approaches and mixes with the deposited material in front of

the barrier, which is also discussed in Wendeler (2008) and Wendeler et al. (2019). This leads to an increase in the depth of flowing layer and part of the dynamic load (momentum) is transferred to the previously deposited layer. As a result of the combination of downward momentum transfer and static load, the lower intermediate cable bears the maximum load.

Evolution of basal stresses and pore fluid pressure

To further explain the load profile on the barrier (Fig. 10), the state of debris flow deposits behind the barrier are analyzed through the measured normal/shear stresses and pore fluid pressure at basal sensing module 2 (Fig. 2a). After each impact, the pore fluid pressure deviates from normal stress, which is the process of pore pressure dissipation. The pore fluid pressure catches up with the normal stress due to the remixing of next surge, indicating that the deposited debris is re-liquefied (Fig. 11). The re-liquefaction is a prerequisite for the downward momentum transfer and the anomalous load profile in Fig. 10.

During the consolidation process of deposited debris with different solid concentrations, the normal stress (red line) generally remains unchanged (Fig. 11). This indicates limited lateral drainage through the net, and solid-liquid separation mainly occurs in the vertical direction. In the impact process, the opening of net is quickly clogged by the well-graded debris material (Fig. 2c), which substantially reduces the permeability of barrier net. This further contradicts the intuition that the highly permeable barrier net enhances the lateral drainage and facilitates to stabilize the deposited debris behind the barrier. On the other hand, comparison between the measured pore fluid pressure (blue line) and the deduced hydrostatic pressure (using the deposited height and water density, green line) indicates that deposits with solid concentration 0.50 and 0.55 remain untrained (with high excessive pore pressure). While deposits with solid concentration 0.40 has been rapidly de-saturated (air entry) after impact. Although de-saturated, due to the high clay content of the debris material, much of the water remains within the deposit as capillary type water, resulting in a minor change in the bulk density and normal stress (Fig. 11a). This also creates the condition for reliquefaction during the re-mixing of subsequent surge impact.

The characteristics of shear stress and pore fluid pressure variation are quite different from the normal stress. As shown in Fig. 11a, the pore fluid pressure of deposited debris with solid concentration 0.40 drops exponentially. The pore fluid pressure with solid concentration of 0.50 rises first and then slowly decreases (Fig. 11b). This is because the consolidation and gradual filling of the subsequent debris occur simultaneously. The latter dominates, causing pore fluid pressure to rise, and then consolidation dominates, causing the pore fluid pressure to slowly dissipate. The shear stress maintains a nearly linear increase, reaching 2 kPa after 3.5 h. The pore fluid pressure with solid concentration of 0.55 decreases in a much lower rate (Fig. 11c). During this period, no significant shear stress is observed, which contradicts with the measurement in Fig. 11b. This is because the deposited debris maintains a nearly liquefied state and therefore the effective grain contact (shear stress) to the flume bed is negligible. As the solid concentration changes from 0.40 to 0.55, the rate of pore fluid pressure dissipation decreases drastically, which reflects the huge difference in the permeability (Iverson and George 2014). Although the inertial-diffusional time scale ratio N_p value in Table 2 only represents the status of pore fluid pressure dissipation of the

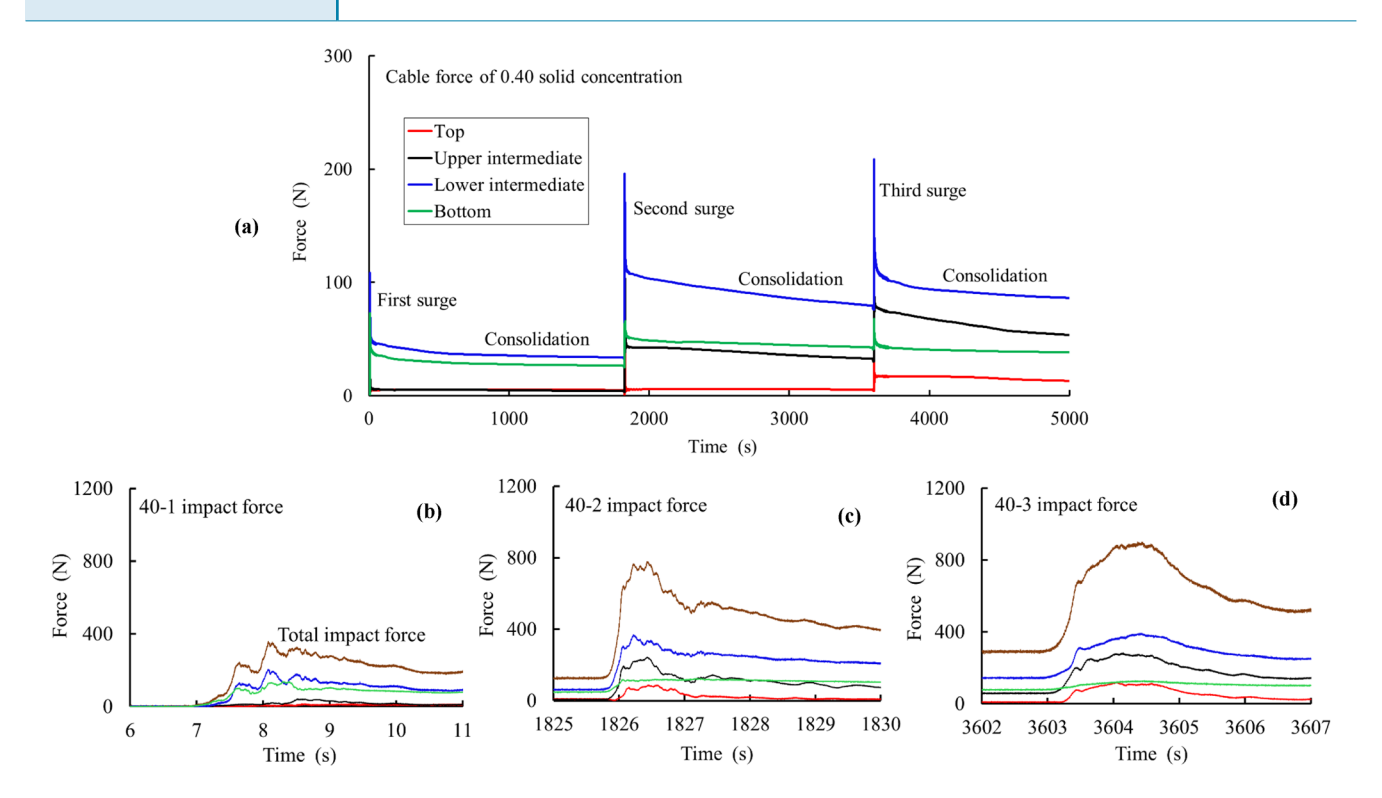


Fig. 6 Measured cable force and calculated normal impact force of 0.40 solid concentration impact. **a** Cable force. **b** Normal impact force of test 40–1. **c** Normal impact force of test 40–3

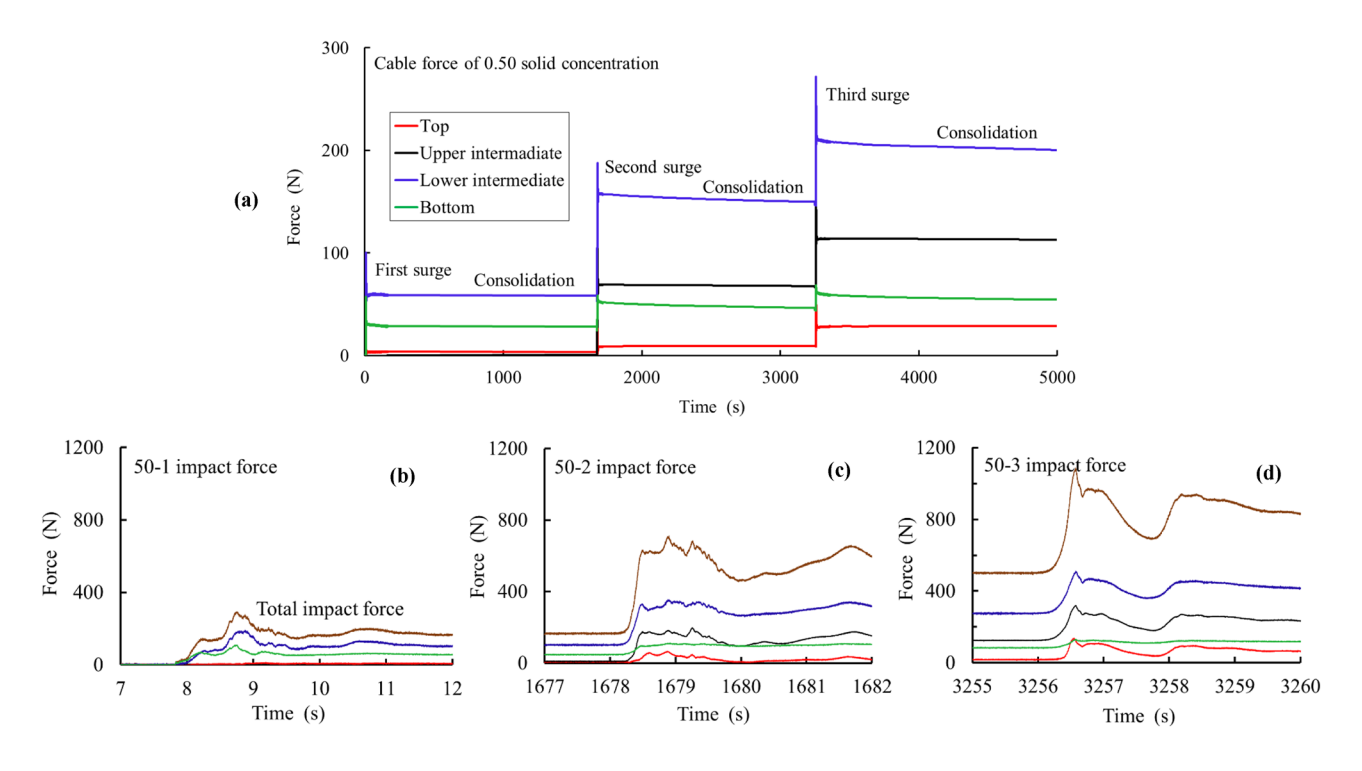
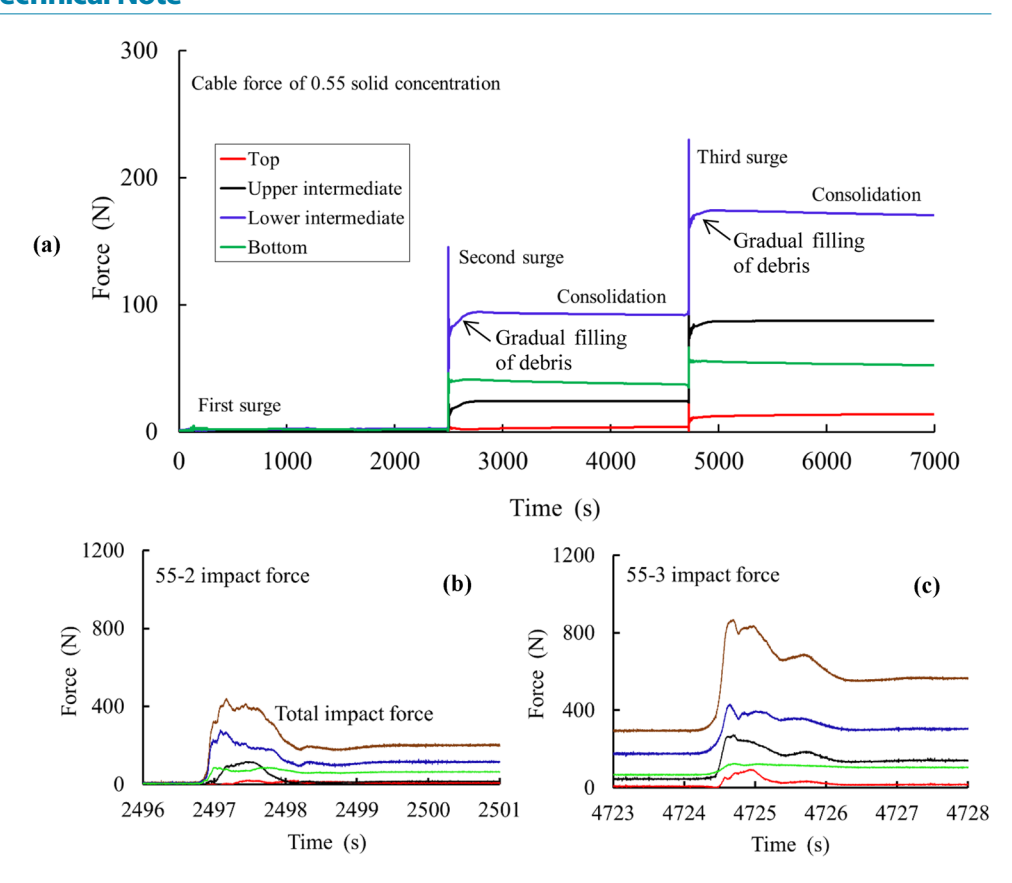


Fig. 7 Measured cable force and calculated normal impact force of 0.50 solid concentration impact. **a** Cable force. **b** Normal impact force of test 50–1. **c** Normal impact force of test 50–2. **d** Normal impact force of test 50–3

Fig. 8 Measured cable force and calculated normal impact force of 0.55 solid concentration impact. **a** Cable force. **b** Normal impact force of test 55–2. **c** Normal impact force of test 55–3



flowing debris, it appears to be a good indicator for the pore fluid dissipation in deposited debris.

Assessment of load model based on the state of deposits

The state of deposited debris reflected by the lateral load on flexible barrier is another important evidence for the cable load profile

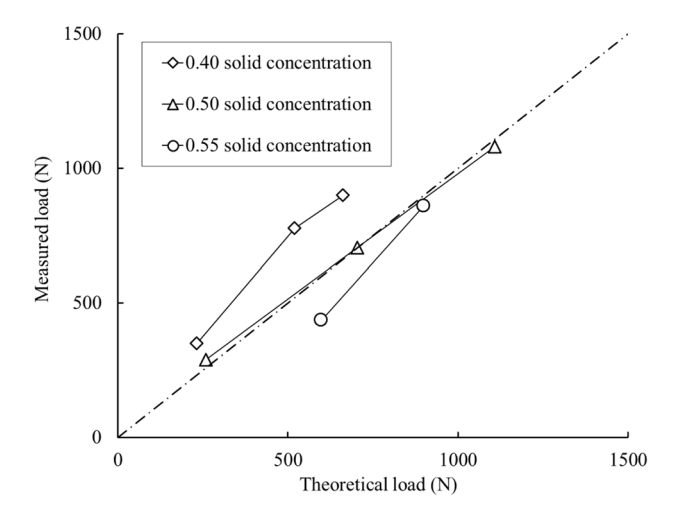


Fig. 9 Comparison between theoretical impact load (with dynamic pressure coefficient α =1.5 and static pressure coefficient k=1) and measured impact load on flexible barrier

(Fig. 10). Figure 12 shows the evolution of static debris load on flexible barrier with three solid concentrations. Owing to the prescribed deformation of horizontal cables, the model flexible barrier is not deformable during impact and consolidation; thus, the state of static debris finally approaches state at rest, rather than an active state for a deformable barrier (Ng et al. 2016; Song et al. 2018). The abscissa represents the state at rest obtained through theoretical calculation, and the ordinate represents the measured lateral load on barrier. The dashed line with "Liquefied k=1" denotes a liquefied state of the debris. The diagonal line with "At rest $k_0 = 0.5$ " denotes the debris is close to the state at rest. Jaky's equation $k_0 = 1 - \sin \varphi$ (Jaky 1944) is adopted to calculate the coefficient of earth pressure at rest, with effective friction angle $\varphi = 30^{\circ}$ for the debris material in this study (Zhou and Ng 2010). The data points of lateral load immediately after the surge impact and right before the next surge impact are adopted. For the last surge impact, data point after 3.5-h consolidation is adopted. For surge impacts with solid concentration 0.40 and 0.50, the data points show a clear zigzag trend. The rise in load denotes that the surge impact increases the total amount of debris behind the barrier, and more importantly, due to the impact induced remixing, the state of debris bends towards the liquefied state (k=1). The drop in load denotes the consolidation process (increase of the grain contact stress) of the debris and the state of debris tends to state at rest ($k_0 = 0.5$). For the two surge impacts with solid concentration 0.55, the low permeability of deposited debris and the gradual filling of subsequent debris material make the zigzag trend unclear.

This remixing (re-liquefaction) process revealed by the state of static deposit (Fig. 12) well explains the downward momentum transfer and the bilinear cable load profile in Fig. 10, which is the

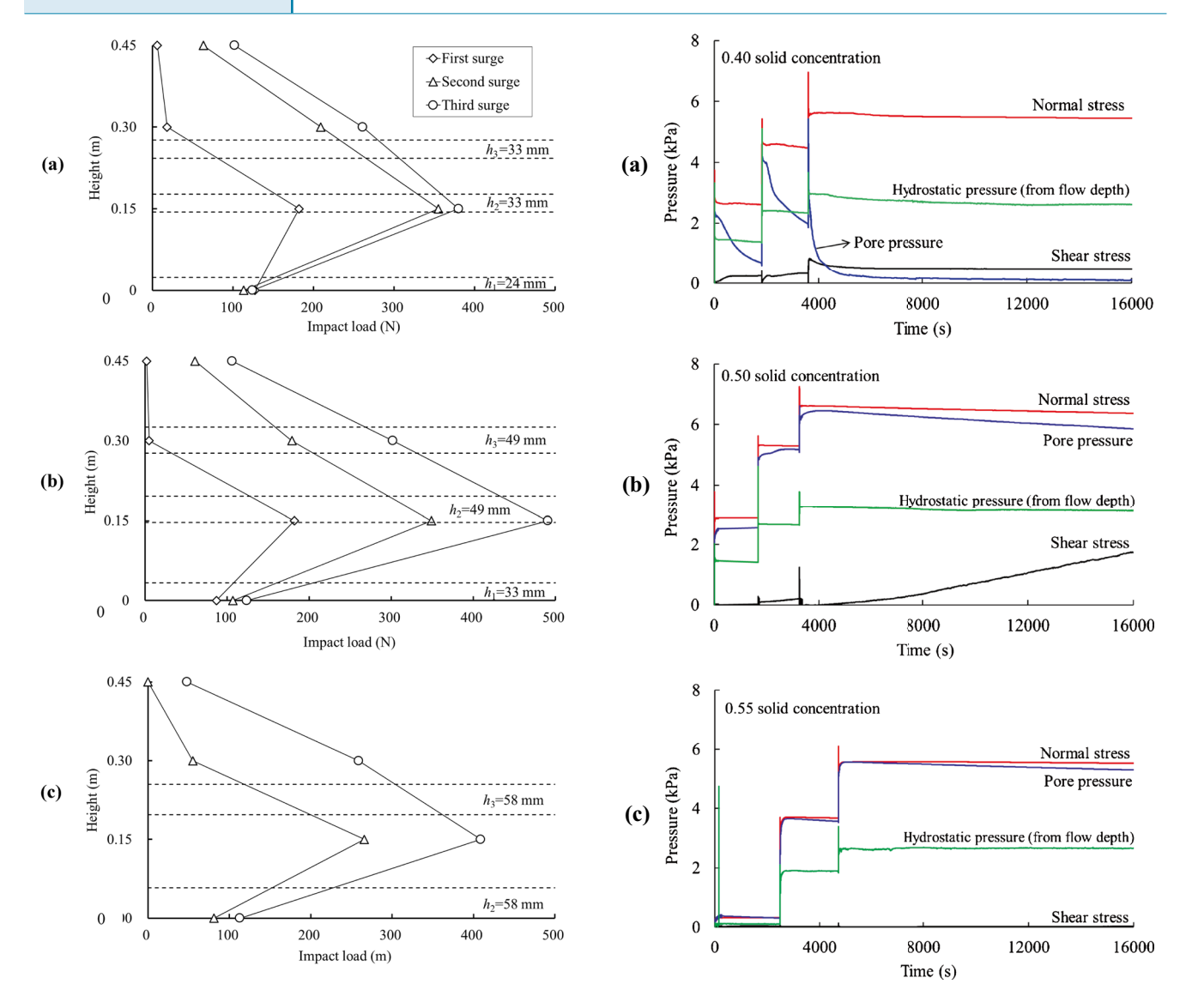


Fig. 10 Cable load profile of normal impact force at the moment of peak value: a 0.40 solid concentration impact; b 0.50 solid concentration impact; and c 0.55 solid concentration impact

key discrepancy between the finding of this study and the multiplesurge load model (Fig. 1). It is noted that, due to the reduced scale of the model tests, the dissipation of pore fluid pressure shall be faster than that in the prototype. Thus, the liquefied state of deposited debris might persist for even longer duration in natural settings. Also, note that the removal of coarse particles (>20 mm) in this study would reduce the intrinsic permeability of debris material, which enhances the time scale of pore fluid pressure dissipation (Eq. 6). Nevertheless, we suggest a detailed site investigation of the fine content of debris source material for debris hazard mitigation, which is the key factor controlling the permeability of solid phase and viscosity of the fluid phase. This would facilitate an accurate estimation of the flow regime (i.e., the inertial-diffusional time scale ratio N_p) and thus to ascertain whether the deposited debris could be remixed by the subsequent surges. Once remixed, the

Fig. 11 Evolution of normal/shear stress and pore fluid pressure at basal sensing module 2: a 0.40 solid concentration; b 0.50 solid concentration; and c 0.55 solid concentration

determination of the cable load (and anchor capacity) along barrier height must be considered with caution.

Conclusions

This experimental study reports a unique set of data of multiple surges impacting a model flexible barrier. By comparing the measurement with the model prediction, the multiple-surge impact model is evaluated from the perspective of total impact load, cable load profile, and state of static deposit. Main conclusions of this study can be drawn as follows:

1. The multiple-surge load model (Kwan 2012; Wendeler et al. 2019) is a remarkable progress in estimating the debris-

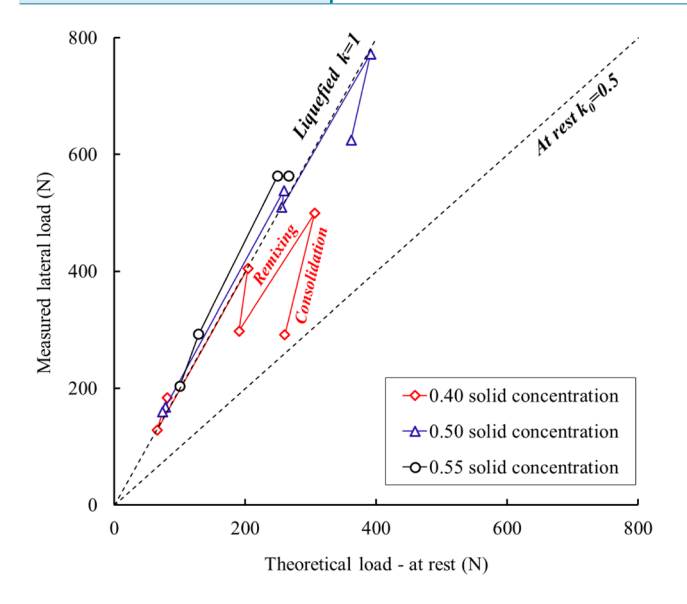


Fig. 12 Evolution of the lateral load on flexible barrier before and after consolidation

flow impact load, since it reflects the physical processes of surge debris impact: the total load is a combination of the static load of preceding as well as current surges and dynamic load of the current surge. In the range of solid concentration 0.40–0.55, the multiple-surge impact load model is reasonable and reliable in predicting the total impact load.

- 2. However, in terms of load profile along barrier height, there is substantial discrepancy between the experimental results and model prediction. Specifically, the impact load concentrates on the lower intermediate cable, rather than the position of flowing debris layer. Analysis of the state of static deposit reveals that the remixing process (interaction between the mobile layer and deposited layer) is the cause of the re-liquefaction of deposited debris and downward momentum transfer to the lower part of barrier.
- 3. Debris flow is usually simplified as single-phase fluid in engineering design. This study reveals that the fundamental physical properties of debris flow are very important for the accurate assessment of debris-flow impact behavior. The amount of fine content in the debris source area affects both the flow mobility and the subsequent impact behavior through reducing permeability and maintaining substantial pore fluid pressure. The inertial-diffusional time scale ratio $N_{\rm p}$ could be a useful index in estimating the impact load of debris flow and evaluating the safety of existing barrier structures.

The simplification of model flexible barrier hinders the direct application of findings of this study to real debris-flow flexible barriers. Specifically, the prescribed deformation in the model barrier makes the response (peak impact load and state of static debris) resemble that of a rigid barrier. Furthermore, the removal of coarse particles modifies the rheology of modelled two-phase debris flow and maintains the pore fluid pressure. Idealized transparent debris materials, i.e., mono-sized spherical glass beads and Newtonian fluid, could be adopted to reveal the fundamental processes of

downward remixing, which is hidden in the opaque slurry. On the other hand, large-scale debris-barrier interaction is warranted to further confirm the findings of this study. More importantly, a physics-based multi-surge impact model with consideration of the downward remixing process would substantially enhance the design of debris-resisting structures.

Acknowledgements

The authors acknowledge the financial support from the National Natural Science Foundation of China (grant No. 41925030, 42077256, and 51809261), the CAS "Light of West China" Program, and the Sichuan Science and Technology Program (grant no. 2020YJ0002). Technical support from the DDFORS (Dongchuan Debris Flow Observation and Research Station) of Chinese Academy of Sciences is also acknowledged.

References

Armanini A, Rossi G, Larcher M (2020) Dynamic impact of a water and sediments surge against a rigid wall. J Hydraul Res 58(2):314–325

Choi CE, Ng CWW, Au-Yeung SCH, Goodwin G (2015) Froude scaling of landslide debris in flume modelling. Landslides 12(6):1197–1206 Cui P, Chen X, Wang Y, Hu K, Li Y (2005) Jiangjia Ravine debris flows in south-western China. In Debris-flow hazards and related phenomena. Springer, Berlin, Heidelberg, pp 565–594

Faug T (2015) Macroscopic force experienced by extended objects in granular flows over a very broad Froude-number range. The European Physical Journal E 38(5):1–10

Fei XJ, Kang ZC, Wang YY (1991) Effect of fine grain and debris flow slurry bodies on debris flow motion. Mountain Research 9(3):143–152 (in Chinese)

GEO (2020) Enhanced technical guidance on design of rigid debris-resisting barriers. Technical Guidance Note No. 52 (TGN 52). Geotechnical Engineering Office, Civil Engineering Department of CEDD, HKSAR

Huang Y, Zhang B (2020) Challenges and perspectives in designing engineering structures against debris-flow disaster. Eur J Environ Civ Eng 1–22

Hübl J, Suda J, Proske D, Kaitna R, Scheidl C (2009) Debris flow impact estimation. In Proceedings of the 11th International Symposium on Water Management and Hydraulic Engineering. Ohrid, Macedonia, pp 1–5

Iverson RM (1997) The physics of debris flows. Rev Geophys 35(3):245-296

Iverson RM (2015) Scaling and design of landslide and debris-flow experiments. Geomorphology 244:9–20

Iverson RM, George DL (2014) A depth-averaged debris-flow model that includes the effects of evolving dilatancy. I. Physical basis. Proc Mathe Phys Eng Sci 470(2170): 20130819

Jaky J (1944) A nyugalmi nyomas tenyezoje (The coefficient of earth pressure at rest). Magyar Mernok es Epitesz-Egylet Kozlonye, pp. 355–358

Kong Y, Li X, Zhao J (2021) Quantifying the transition of impact mechanisms of geophysical flows against flexible barrier. Eng Geol 106188

Kwan JSH (2012) Supplementary technical guidance on design of rigid debris-resisting barriers. GEO Report No. 270. Geotechnical Engineering Office, HKSAR Government

Li XY, Zhao J (2018) A unified CFD-DEM approach for modeling of debris flow impacts on flexible barriers. Int J Numer Anal Meth Geomech 42(14):1643–1670

Nagl G, Hübl J, Kaitna R (2020) Velocity profiles and basal stresses in natural debris flows. Earth Surf Proc Land 45(8):1764–1776

Ng CWW, Song D, Choi CE, Koo RCH, Kwan JSH (2016) A novel flexible barrier for landslide impact in centrifuge. Géotechnique Letters 6(3):221–225

- Pudasaini SP (2012) A general two-phase debris flow model. J Geophys Res Earth Surf 117(F3)
- Rickenmann D (1999) Empirical relationships for debris flows. Nat Hazards 19:47–77
- Savage SB (1984) The mechanics of rapid granular flows. Adv Appl Mech 24:289–366
- Shi QY, Tang C, Gong LF, Chen M, Li N, Zhou W, Xiong J, Tang H, Wang XD, Li MW (2021) Activity evolution of landslides and debris flows after the Wenchuan earthquake in the Qipan catchment, Southwest China. J Mt Sci 18(4):932–951
- Song D, Ng CWW, Choi CE, Zhou GGD, Kwan JSH, Koo RCH (2017) Influence of debris flow solid fraction on rigid barrier impact. Can Geotech J 54(10):1421–1434
- Song D, Choi CE, Ng CWW, Zhou GGD (2018) Geophysical flows impacting a flexible barrier: effects of solid-fluid interaction. Landslides 15(1):99–110
- Song D, Choi CE, Ng CWW, Zhou GGD, Kwan JSH, Sze HY, Zheng Y (2019a) Load-attenuation mechanisms of flexible barrier subjected to bouldery debris flow impact. Landslides 16(12):2321–2334
- Song D, Zhou GGD, Xu M, Choi CE, Li S, Zheng Y (2019b) Quantitative analysis of debris-flow flexible barrier capacity from momentum and energy perspectives. Eng Geol 251:81–92
- Song D, Zhou GGD, Chen XQ, Li J, Wang A, Peng P, Xue KX (2021a) General equations for landslide-debris impact and their application to debris-flow flexible barrier. Eng Geol 288: 106154
- Song D, Chen X, Zhou GGD, Lu X, Cheng G, Chen Q (2021b) Impact dynamics of debris flow against rigid obstacle in laboratory experiments. Eng Geol 261:106211
- Tan DY, Yin JH, Qin JQ, Zhu ZH, Feng WQ (2020) Experimental study on impact and deposition behaviours of multiple surges of channelized debris flow on a flexible barrier. Landslides 17(7):1577–1589
- Wendeler C (2008) Murgangrückhalt in Wildbächen Grundlagen zu Planung und Berechnung von flexiblen Barrieren, Diss. ETH Nr. 17916
- Wendeler C, Volkwein A, McArdell BW, Bartelt P (2019) Load model for designing flexible steel barriers for debris flow mitigation. Can Geotech J 56(6):893–910
- Wendeler C, Budimir V, Denk M (2018) Debris flow protection with flexible ring net barriers–10 years of experience. In: Proceedings of the 16th Danube-European Conference on Geotechnical Engineering 2(2–3): 1039–1044
- Wendeler C, Volkwein A, Denk M, Roth A, Wartmann S (2007) Field Measurements Used for Numerical Modelling of Flexible Debris Flow Barriers. In: Chen CL, Major JJ (eds) Proceedings of Fourth International Conference on Debris Flow Hazards Mitigation: Mechanics, Prediction, and Assessment, 10–13. Chengdu, China, pp 681–687
- Yang HJ, Hu KH, Wei FQ (2013) Methods for computing rheological parameters of debris-flow slurry and their extensibilities. Shuili Xuebao 44(11):1338–1346 (in Chinese)

- Zanuttigh B, Lamberti A (2007) Instability and surge development in debris flows. Rev Geophys 45(3)
- Zhou GGD, Ng CWW (2010) Dimensional analysis of natural debris flows. Can Geotech J 47(7):719–729
- Zhou GGD, Song D, Choi CE, Pasuto A, Sun QC, Dai DF (2018) Surge impact behavior of granular flows: effects of water content. Landslides 15(4):695–709

Supplementary Information The online version contains supplementary material available at https://doi.org/10.1007/s10346-021-01778-3.

Dongri Song · Yitong Bai · Xiao Qing Chen (⊠) · Gordon G. D. Zhou

Key Laboratory of Mountain Hazards and Earth Surface Process, Institute of Mountain Hazards and Environment, Chinese Academy of Sciences (CAS), Chengdu, China Email: xqchen@imde.ac.cn

Dongri Song · Yitong Bai · Xiao Qing Chen · Gordon G. D. Zhou

University of Chinese Academy of Sciences, Beijing, China Email: drsong@imde.ac.cn

Yitong Bai

Email: baiyitong18@mails.ucas.ac.cn

Gordon G. D. Zhou

Email: gordon@imde.ac.cn

Gordon G. D. Zhou

China-Pakistan Joint Research Center on Earth Sciences, CAS-HEC, Islamabad, Pakistan Email: gordon@imde.ac.cn

Clarence E. Choi

Department of Civil Engineering, University of Hong Kong, Hong Kong SAR, China Email: cechoi@hku.hk

Alessandro Pasuto

Research Institute for Geological and Hydrological Hazard Prevention, National Research Council of Italy, Padova, Italy Email: alessandro.pasuto@irpi.cnr.it

Peng Peng

PowerChina HuaDong Engineering Corporation Limited, Hangzhou, China

Email: peng_p@ecidi.com